Gas Permeation Properties of Poly(1,1′-dihydroperfluorooctyl acrylate), Poly(1,1′-dihydroperfluorooctyl methacrylate), and Poly(styrene)-*b*-poly(1,1′-dihydroperfluorooctyl acrylate) Block Copolymers

Michelle E. Arnold, Kazukiyo Nagai,† Benny D. Freeman,* and Richard J. Spontak

Department of Chemical Engineering, North Carolina State University, Raleigh, North Carolina 27695-7905

Douglas E. Betts‡ and Joseph M. DeSimone§

Department of Chemistry, University of North Carolina at Chapel Hill, Chapel Hill, North Carolina 27599-3290

Ingo Pinnau

Membrane Technology and Research, Inc., 1360 Willow Road, Suite 103, Menlo Park, California 94025-1516

Received February 27, 2001; Revised Manuscript Received May 17, 2001

ABSTRACT: The permeabilities of rubbery poly(1,1′-dihydroperfluorooctyl acrylate) (PFOA), glassy poly(1,1′-dihydroperfluorooctyl methacrylate) (PFOMA), and poly(styrene)-*b*-poly(1,1′-dihydroperfluorooctyl acrylate) (PS-*b*-PFOA) diblock copolymers to N_2, O_2, H_2, CH_4, C_2H_6, and CO_2 at 446 kPa and to C_3H_8 at 308 kPa are reported as a function of temperature. In general, PFOMA has lower fractional free volume, smaller gas permeability coefficients, and larger activation energies of permeation than PFOA, consistent with the more restricted long-range segmental mobility of PFOMA. The PS-*b*-PFOA copolymers exhibit complex microphase-separated morphologies, and their gas permeability coefficients are intermediate between those of glassy PS and rubbery PFOA, decreasing in magnitude with increasing PS content.

Introduction

Typically, fluoropolymers have high thermal, chemical, and oxidative stability, which suggests that they could be attractive membrane materials for separations in chemically challenging environments, such as vapor separation or removal of perfluorocarbons from waste streams containing hydrofluoric acid. Traditionally, however, fluoropolymers have been synthesized and processed in solvents such as chlorofluorocarbons (CFCs) and halocarbons, which are deleterious to the environment.[1−3] To address this problem, DeSimone and coworkers[1,4] have developed methods for the synthesis of fluoropolymers in supercritical carbon dioxide ($scCO_2$). Two chemically related fluoropolymers—poly(1,1′-dihydroperfluorooctyl acrylate) (PFOA) and poly(1,1′-dihydroperfluorooctyl methacrylate) (PFOMA)—have been synthesized in $scCO_2$ for this study, and their chemical structures are presented in Figure 1. At ambient temperature, PFOA is a rubbery polymer with a glass transition temperature, T_g, of −10 °C,[5] while PFOMA is a glassy polymer with a T_g of 50 °C.

Block copolymers offer an extra degree of freedom in tailoring polymer properties.[6,7] Only a limited number of gas permeation studies employing block copolymers have been reported in the literature.[8−18] This work describes the permeation and morphological characteristics of a series of microphase-separated poly(styrene)-*b*-poly(1,1′-dihydroperfluorooctyl acrylate) (PS-*b*-PFOA)

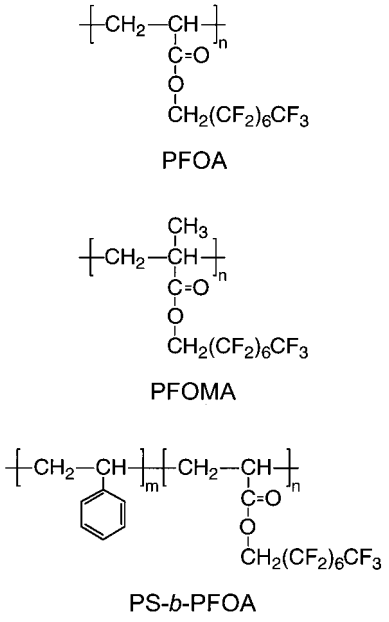

Figure 1. Chemical structures of the poly(1,1′-dihydroperfluorooctyl acrylate) (PFOA) and poly(1,1′-dihydroperfluorooctyl methacrylate) (PFOMA) homopolymers as well as the poly(styrene-*b*-1,1′-dihydroperfluorooctyl acrylate) (PS-*b*-PFOA) diblock copolymers.

* To whom correspondence should be addressed.
† Present address: CSIRO Molecular Science, Private Bag 10, Clayton South, VIC 3169, Australia.
‡ Present address: Nalco Chemical Company, One Nalco Center, Naperville, IL 60563-1198.
§ Also affiliated with Department of Chemical Engineering, North Carolina State University, Raleigh, NC 27695-7905.

10.1021/ma010355i CCC: $20.00
Published on Web 07/06/2001

diblock copolymers and compares them with the properties of the constituent homopolymers, PFOA and PS, and with those of a structurally related fluoropolymer, PFOMA.

Background

Transport Fundamentals. The permeability, P, of a polymer film of thickness l to a penetrant is[19]

$$P = \frac{Nl}{p_1 - p_2} \tag{1}$$

where N is the steady-state penetrant flux, and p_1 and p_2 denote the upstream and downstream penetrant partial pressures, respectively. Permeation through dense, nonporous polymer films is conventionally described by the solution-diffusion model,[20] in which penetrant molecules first sorb into the upstream face of the film, diffuse through the polymer matrix, and then desorb from the downstream face of the film. The rate-limiting step in this process is diffusion across the polymer film. Within the context of this transport model and when $p_2 \ll p_1$, permeability is given by[19]

$$P = DS \tag{2}$$

where D is the concentration-averaged effective diffusion coefficient, and S is the apparent solubility coefficient (i.e., the ratio of the dissolved penetrant concentration in the upstream face of the film to the upstream penetrant partial pressure in the contiguous gas phase). A measure of the ability of a polymer matrix to separate gaseous penetrants is given by the ideal selectivity for penetrant A relative to penetrant B (α_{AB}):[19]

$$\alpha_{AB} = \frac{P_A}{P_B} \tag{3}$$

where P_A and P_B are the permeability coefficients of species A and B, respectively.

Effect of Temperature on Permeability. Permeability coefficients usually obey an Arrhenius relationship:[19]

$$P = P_0 e^{-E_P/RT} \tag{4}$$

where P_0 is a constant, E_P is the activation energy of permeation, R is the universal gas constant, and T denotes absolute temperature. If the temperature range of interest is sufficiently far from thermal transitions (e.g., melting, glass−rubber or order−disorder), then E_P is usually independent of temperature. Because permeation includes both diffusion and solution steps, the activation energy of permeation is written as[19]

$$E_P = E_D + \Delta H_s \tag{5}$$

where E_D is the activation energy of diffusion, which describes the energy required to create a diffusion gap of sufficient size to accommodate a penetrant molecule.[21] The overall enthalpy of sorption, ΔH_s, is frequently written in terms of two contributions:[19]

$$\Delta H_s = \Delta H_{cond} + \Delta H_{mix} \tag{6}$$

where ΔH_{cond} is the enthalpy of condensation for the pure penetrant and ΔH_{mix} is the enthalpy required for mixing the penetrant and polymer segments.

Experimental Section

Materials. High-molecular-weight PFOA and PFOMA were synthesized in $scCO_2$ as previously described by Guan et al.[4] Homogeneous free-radical solution polymerization of a fluorinated monomer (e.g., 1,1′-dihydroperfluorooctyl acrylate, FOA) was typically conducted in the presence of 1 wt % azoisobutyronitrile (AIBN) as initiator at 59.4 °C and 207 bar for 48 h.[4] The FOA and FOMA monomers were graciously provided by 3M Co. (Minneapolis, MN), and styrene monomer was purchased from Aldrich Chemical Co. (Milwaukee, WI). The PS-*b*-PFOA copolymers were synthesized by an iniferter process,[5,22,23] in which telechelic polystyrene was first produced using tetraethylthiuram disulfide as the thermal iniferter and characterized. The PFOA block was subsequently polymerized using the telechelic PS as a macroinitiator.[5,24]

Nitrogen, O_2, H_2, CH_4, C_2H_6, C_3H_8, and CO_2 were obtained from National Specialty Gases (Raleigh, NC) and were used as received. The minimum purity of each gas was 99.998 mol % for N_2, 99.8 mol % for H_2, 99.5 mol % for O_2 and CO_2, and 99 mol % for CH_4, C_2H_6, and C_3H_8. In addition, 1,1,2-trichlorotrifluoroethane (Freon-113), used to cast films and prepare composite membranes, was acquired from E.I. DuPont de Nemours and Co. (Wilmington, DE).

Polymer Characterization. For the PS-*b*-PFOA block copolymers, molecular weights for the telechelic polystyrenes were first measured using a Waters 150-CV gel permeation chromatograph equipped with Ultrastyragel columns of 10, 50, 100, and 1000 nm porosities. Tetrahydrofuran was the eluent, and the instrument was calibrated using PS standards from Showa Denko (Tokyo, Japan).[24] The number of *N*,*N*-diethyldithiocarbamate end groups per polymer chain (i.e., the functionality) of each telechelic polystyrene was ascertained from UV spectrophotometry results acquired using a Perkin-Elmer Lambda 6 UV−vis spectrophotometer.[24] Composition analysis of the PS-*b*-PFOA block copolymers was conducted with proton nuclear magnetic resonance (^{1}H NMR) using a Bruker WM 250 spectrometer.[24] These measurements were performed in a mixed solvent of Freon-113 and either d_2-methylene chloride or d_6-acetone. Subsequently, PFOA block weights were determined using the ratio of the fluorinated block peak to the PS block peak and the known molecular weight of the PS block.[24]

Glass transition temperatures were characterized by differential scanning calorimetry (DSC), using a Perkin-Elmer DSC-7 calorimeter operated at a heating rate of 20 °C/min in a N_2 atmosphere. The density of PFOA was determined from pycnometric analysis, in which the masses and volumes of PFOA films cast from a 20% (w/v) solution in Freon-113 were measured after complete solvent evaporation (quiescent drying at ambient temperature for 3 weeks, followed by vacuum-drying at ambient temperature for 3 days). The density of PFOMA was ascertained by gravimetric analysis, in which PFOMA films measuring ca. 200 μm thick were prepared from similar Freon-113 solutions using a ring-casting technique.[25] Following complete solvent evaporation, the density of PFOMA was estimated from the masses and dimensions of uniform circular PFOMA samples (1.90 cm in diameter).

Morphological Characterization. Electron-transparent specimens for transmission electron microscopy (TEM) were prepared by casting PS-*b*-PFOA films from 5% (w/v) Freon-113 solutions in Teflon molds, followed by slow solvent evaporation. Dried films measuring 0.3−0.6 mm thick were subsequently microtomed at −100 °C in a Reichert-Jung Ultracut-S cryoultramicrotome, and the resultant thin sections were exposed to the vapor of 2% RuO_4(aq) for 5 min to stain the PS-rich microdomains. Images were acquired with a Zeiss EM902 electron spectroscopic microscope operated at 80 kV and energy-loss settings of 0−180 eV. Correlation lengths were discerned from 2D Fourier transforms of digitized negatives using the Digitalmicrograph software package by Gatan Inc. (Pleasanton, CA).

Table 1. Physical Properties of the Polymers Investigated in This Study

	ϕ_S	T_g (°C)	$\bar{M}_n \times 10^{-3}$ PS	PFOA	PFOMA	density (g/cm^3)
PFOA	0.0	−10		>10^3		1.74
PS-*b*-PFOA	0.12	−6/66	14.0	172		
PS-*b*-PFOA	0.23	−3/67	4.5	24.5		
PS-*b*-PFOA	0.03	−7/69	6.60	349		
PS	1.0	100[a]	>10^3			1.06[a]
PFOMA		50			>10^3	1.89

[a] Reference 50.

Composite membranes were prepared by coating 1−2% (w/v) Freon-113 solutions onto a highly microporous polysulfone (PSF) support with a nonwoven polyester backing. Thin strips of the composite membranes for scanning electron microscopy (SEM) were cut from areas adjacent to those used for permeation testing. The strips were soaked in ethanol for 1−5 min to swell and open the microporous structure of the PSF support. After the polyester backing was removed, each sample was fractured in liquid nitrogen. The resultant cross sections were mounted and sputter-coated with ca. 20 nm of Au, and backscattered electron images were acquired at 20 kV with a Hitachi S-3200N variable-pressure electron microscope. The separating layer thickness for each composite membrane was estimated on the basis of SEM analysis and represents the average of multiple measurements collected from several samples of each membrane.

Permeation Measurements. Pure gas permeability coefficients of composite membranes were determined using a constant pressure/variable volume method.[26] The feed-side (upstream) pressure was maintained at 446 kPa (50 psig) for all penetrant gases except C_3H_8, which was tested at 308 kPa (30 psig), while the permeate-side (downstream) pressure was atmospheric. Permeation measurements were conducted in ca. 5 °C intervals for temperatures ranging from ambient (23 °C) to 45 °C, and temperature was maintained within ±0.5 °C with a DYNA-SENSE temperature control system (Cole-Palmer, Niles, IL). At each temperature, the typical order of permeation measurements was N_2, O_2, H_2, CH_4, C_2H_6, C_3H_8, CO_2, N_2, O_2. After the fluxes for all penetrant gases were determined at each temperature, the temperature was decreased back to 23 °C, and the fluxes for N_2, O_2, and at least one other penetrant (typically C_2H_6 or C_3H_8) were measured again. Permeate flow rates were determined using a soap film bubble flowmeter from Alltech (Deerfield, IL). Once steady-state conditions were established, the pure gas permeability coefficient, P, was estimated from

$$P = \frac{l}{A(p_1 - p_{atm})} \frac{273\ \text{K}}{T} \frac{p_{atm}}{76\ \text{cm Hg}} \left(\frac{dV}{dt}\right)_{ss} \quad (7)$$

where l is the estimated effective separating layer thickness of the membrane (cm), A is the membrane area (cm^2), p_{atm} is atmospheric pressure (cmHg), p_1 is the upstream pressure (cmHg), T is absolute temperature (K), and $(dV/dt)_{ss}$ is the steady-state volumetric rate of soap-bubble displacement in the flowmeter (cm^3/s). All permeability coefficients are reported in units of barrers, where 1 barrer = 10^{-10} cm^3 (STP)·cm/(cm^2·s·cmHg).

Results and Discussion

Physical Property Characterization. The physical properties of PFOA, PFOMA, and PS homopolymers, as well as three PS-*b*-PFOA diblock copolymers, are recorded in Table 1. High-molecular-weight PFOA is a rubbery polymer with a T_g of −10 °C. In contrast, PFOMA is a glassy polymer with a T_g of 50 °C. The difference in T_g is attributed to the additional methyl group in the PFOMA backbone. Each of the PS-*b*-PFOA copolymers has two T_g values, which is a signature of microphase separation.[27] The lower T_g is associated with the glass transition of chain segments in the PFOA-rich microdomains, while the higher T_g is ascribed to the glass transition of PS-rich microdomains. The T_g associated with the PFOA-rich phase is a few degrees higher than that of pure PFOA, and the T_g associated with the PS-rich phase is 31−34 °C lower than that of pure PS. Differences between the T_g's of the copolymer blocks and those of the parent homopolymers can be attributed to three effects. Interfacial mixing between PS and PFOA microdomains promotes convergence of the two T_g's (until a single T_g would be achieved upon microphase dissolution). Incomplete microphase separation in which the PS microdomains contain PFOA due to kinetic entrapment or polydispersity effects[28] results in residual intramicrodomain mixing and is accompanied by a depression in the T_g associated with the PS-rich phase. In addition, the T_g of a relatively short homopolymer or copolymer block depends sensitively on molecular weight. Lu and Jiang[29] have proposed the following correlation between the T_g of PS and the degree of polymerization (N_S):

$$T_g = \frac{2N_s T_g^\infty}{2N_s + C_\infty f(y)} \quad (8)$$

where T_g^∞ = 373.15 K and C_∞ = 10.68 for PS. The function $f(y)$ is obtained from the wormlike chain model and is given by

$$f(y) = 1 - 3y + 6y^2 - 6y^3(1 - e^{-1/y}) \quad (9)$$

For a vinyl polymer chain,

$$y = \frac{C_\infty}{4N_s \sin^2(\theta/2)} \quad (10)$$

where θ is the angle formed by the C−C single bonds along the backbone (109.5°). On the basis of this model, the T_g values of the PS blocks with $\bar{M}_n$ equal to 14 000, 4500, and 6600 (see Table 1) would be 87, 68, and 76 °C, respectively. Differences between these calculated T_g's and the experimental T_g's, particularly for the samples containing PS blocks of molecular weight 14 000 and 6600, suggest that PS segment molecular weight is insufficient to explain the large depression in glass transition temperatures of the PS in these block copolymers. Therefore, interfacial and/or residual intramicrodomain mixing may also contribute to the reduced T_g values. This issue is revisited later in the discussion.

The densities of PFOA and PFOMA are also included in Table 1. The density of PFOA is 1.74 g/cm^3, which is essentially equal to that of TFE/BDD87, a glassy, random perfluorodioxole copolymer prepared from 13 mol % tetrafluoroethylene and 87 mol % 2,2-bis(trifluoromethyl)-4,5-difluoro-1,3-dioxole.[30] In contrast, the density of PFOMA, 1.89 g/cm^3, lies between that of TFE/BDD87 and poly(tetrafluoroethylene) (2.15−2.20 g/cm^3).[31] The measured densities of PFOA and PS provided in Table 1 are used in conjunction with the known mass-fraction compositions of the PS-*b*-PFOA copolymers (from ^{1}H NMR) to estimate volume fractions of PS (ϕ_S). Insufficient quantities of the PS-*b*-PFOA copolymer samples were available for density determination.

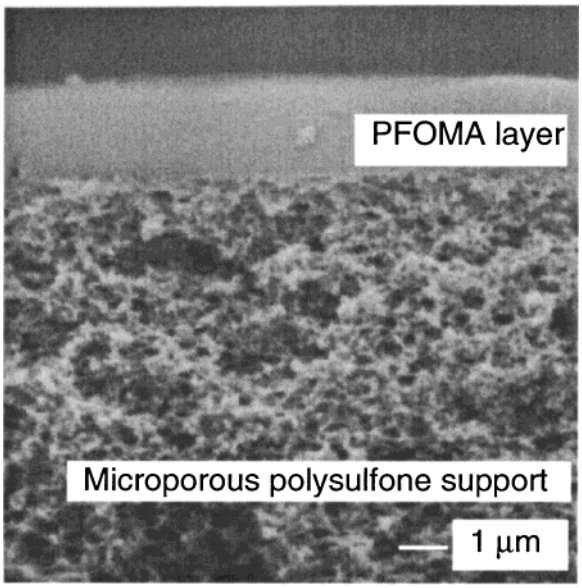

Figure 2. Scanning electron micrograph of a PFOMA composite membrane used for gas permeability measurements. The PFOMA separating layer is approximately 2.1 μm thick and is coated onto a highly microporous polysulfone support.

Table 2. Pressure-Normalized Fluxes of PFOA and PFOMA at Ambient Temperature, 446 kPa Feed Pressure, and 101 kPa Permeate Pressure

		pressure-normalized flux (GPU)[a]						
	FFV[b]	N_2	O_2	H_2	CH_4	C_2H_6	C_3H_8[c]	CO_2
PFOA	0.24	32	74	177	34	40	57	310
PFOMA	0.13	7	18	41	7	6	6	63

[a] 1 GPU = 10^{-6} cm^3 (STP)/(cm^2·s·cmHg). [b] Estimated by a group contribution method.[34] [c] C_3H_8 data were collected at a feed pressure of 308 kPa and a permeate pressure of 101 kPa.

Permeation Properties of PFOA and PFOMA. A representative SEM image of the cross section of a thin-film composite membrane is shown in Figure 2. The lower region corresponds to the microporous PSF support, while the upper region is a PFOMA film with an apparent thickness of 2.1 μm. Pure-gas pressure-normalized fluxes for PFOA and PFOMA at ambient temperature (23 °C) are recorded in Table 2. The estimated uncertainty in these values is less than 10% based on a propagation of error analysis. Permeability coefficients have been determined from the data in Table 2 by assuming that the effective separating layer thickness of each membrane was equal to the separating layer thickness estimated by SEM analysis and are provided in Table 3. Partial penetration of the polymeric separating layer into the microporous substructure of the composite membrane support could affect the magnitude of the effective separating layer thickness; however, we did not observe significant penetration into the membrane support by SEM. Additionally, it was impossible to prepare free-standing films of PFOA or sufficiently large films of PFOMA for permeation testing. The estimated experimental error for all permeability coefficients is less than 20% based on a propagation of error analysis.[32]

Gas permeability coefficients are lower and ideal gas selectivities are higher in PFOMA than in PFOA. Free volume is an important factor influencing diffusion and, consequently, permeation.[33] Based on Bondi's group contribution method, estimated fractional free volume (FFV) values for PFOA and PFOMA are 0.24 and 0.13, respectively.[34] The lower gas permeability coefficients in PFOMA relative to PFOA are consistent with the lower FFV and more restricted chain mobility of PFOMA. Table 3 also shows that permeability values for PFOA and PFOMA seemingly lie between those of TFE/BDD87 and PTFE. Due in part to its high FFV (0.33 based on a density of 1.74 g/cm^3),[35] TFE/BDD87 is the most permeable fluoropolymer known. In contrast, PTFE is highly crystalline, and the estimated FFV for a hypothetical, fully amorphous sample is 0.23.[34,36] Although the estimated FFVs of PFOA and PTFE are comparable, PFOA permeability coefficients are larger than those of PTFE. This trend may reflect two main differences in physical properties. PFOA is amorphous, whereas PTFE is semicrystalline, and crystalline regions in polymers typically act as impermeable barriers to gas transport.[37] Additionally, the long-range segmental motion of PFOA chains is expected to be greater than PTFE because its T_g is more than 100 °C lower than that of PTFE (115−140 °C).[38]

Figure 3 presents the dependence of permeability on penetrant critical volume, a convenient measure of penetrant size. Permeability coefficients for light gases in PFOMA and PFOA decrease in the same order:

$$CO_2 > H_2 > O_2 > N_2 \approx CH_4$$

For rubbery PFOA, hydrocarbon permeability coefficients increase slightly with increasing penetrant size:

$$CH_4 < C_2H_6 < C_3H_8$$

As hydrocarbon number increases, solubility typically increases, which acts to increase permeability, and diffusivity should decrease, which acts to decrease permeability.[33] Many rubbery polymers, such as PFOA and poly(dimethylsiloxane) (PDMS), sieve penetrants weakly on the basis of size,[39] and hence, permeability increases with increasing solubility. In contrast, hydrocarbon permeability coefficients are much lower in PFOMA than in PFOA. In PFOMA, they are nearly independent of hydrocarbon penetrant size, suggesting that PFOMA presents a more strongly size sieving matrix to the penetrants than PFOA, albeit much weaker than that of PS.

Ideal gas selectivities for O_2/N_2 and CO_2/CH_4 are presented in Table 3. For all the fluoropolymers, selectivity decreases as permeability increases. This result is consistent with the well-known tradeoff[40,41] between permeability and selectivity: more permeable polymers are generally less selective and vice versa. Polymers with the best combinations of permeability and selectivity lie on the "upper bound" tradeoff curve. Robeson[40] developed quantitative relations for estimating the upper bound limit of selectivity from experimentally determined permeability coefficients. Table 3 reports the calculated upper bound selectivities. All experimental ideal gas selectivities for PFOA and PFOMA are lower than the calculated upper bound values. The O_2/N_2 selectivity for PFOMA is 48% of the calculated upper bound selectivity. The O_2/N_2 and CO_2/CH_4 selectivities for PFOA are 60% and 50% of the upper bound limits, respectively. These values are closer to the upper bound selectivities than those for other gas pairs studied, i.e., H_2/CH_4, H_2/N_2, and H_2/O_2. In comparison, the ideal pure gas O_2/N_2 selectivities for TFE/BDD87,[35] polysulfone,[42] and PDMS[42] are 77%, 64%, and 62%, respectively, of the calculated upper bound values. These results sug-

Table 3. Gas Permeability Coefficients and Selectivity Values of Selected Fluoropolymers at Ambient Temperature, 446 kPa Feed Pressure, and 101 kPa Permeate Pressure

		permeability coefficient (barrers)[a]							selectivity			
									O_2/N_2		CO_2/CH_4	
	FFV[b]	N_2	O_2	H_2	CH_4	C_2H_6	C_3H_8[c]	CO_2	exptl	calcd[d]	exptl	calcd[d]
TFE/BDD87[e]	0.33	780	1600	3400	600	370	200	3900	2.0	2.6	6.5	8.5
PFOA[f]	0.24	54	130	300	57	68	97	520	2.4	4.0	9.1	18
PFOMA[f]	0.13	15	36	82	14	13	12	130	2.4	5.0	9.1	31
PTFE[g]	0.16	1.3	4.2	9.8	0.74			10	3.2	7.2	13.4	82

[a] 1 barrer = 10^{-10} cm^3(STP)·cm/(cm^2·s·cmHg). [b] Estimated by a group contribution method.[34] [c] C_3H_8 data were collected at a feed pressure of 308 kPa and a permeate pressure of 101 kPa. [d] Calculated from Robeson's correlation:[40] separation factor = $(P_i/k)^{1/n}$ where k = 389 224 and 1 073 700 barrers and n = −5.8000 and − 2.6264 for O_2/N_2 and CO_2/CH_4, respectively. [e] Reference 35. [f] Based on separating layer thicknesses of 1.7 ± 0.3 and 2.0 ± 0.1 μm for PFOA and PFOMA, respectively. [g] This value is the estimated FFV for a hypothetical, fully amorphous sample.[36]

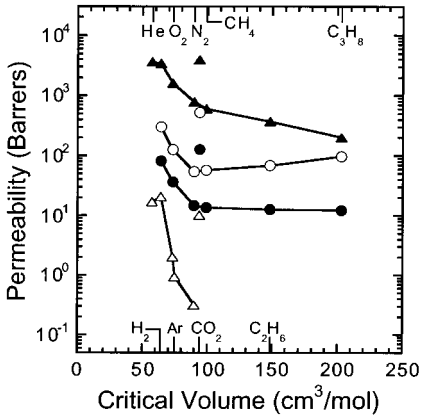

Figure 3. Gas permeability coefficients in PFOA (○), PFOMA (●), PS[50] (△), and TFE/BDD87[35] (▲) at ambient temperature as a function of penetrant critical volume.

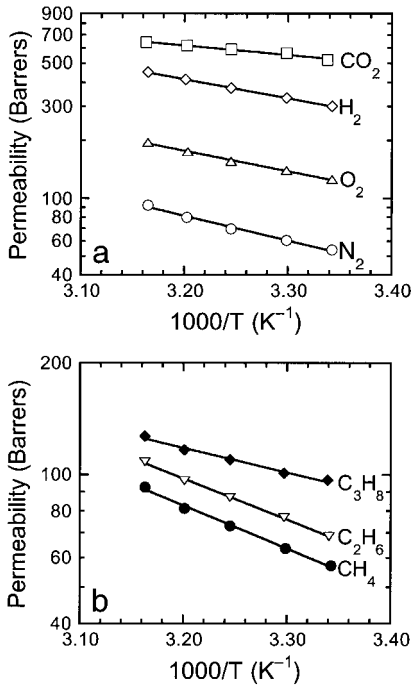

Figure 4. Temperature dependence of gas permeability coefficients for (a) permanent gases and (b) hydrocarbons in PFOA. Shown in (a) are permeability coefficients for N_2 (○), O_2 (△), H_2 (◇), and CO_2 (□). The coefficients for CH_4 (●), C_2H_6 (▽), and C_3H_8 (◆) are displayed in (b). Solid lines correspond to least-squares fits of eq 4 to the data.

gest that PFOMA and PFOA are not attractive materials for industrial gas separations.

Temperature Dependence of Permeability. Figure 4 illustrates the temperature dependence of gas permeability in PFOA. The permeability coefficients obey the Arrhenius relation over the temperature range of this study. The temperature dependence of permeability for permanent gases and hydrocarbons in PFOMA is presented in parts a and b of Figure 5, respectively. The Arrhenius plots for the permanent gases in Figure 5a are nearly linear over the entire temperature range tested. However, the corresponding plots for C_2H_6 and C_3H_8 in Figure 5b are not linear. Since the T_g of PFOMA is 50 °C, which is near the upper limit of temperatures explored in this study, this apparent nonlinear behavior is attributed to the permeation measurements of these large penetrants being conducted near T_g. These results are consistent with the diffusion results reported by Kumins and Roteman[43] for a random poly(vinyl chloride-*co*-vinyl acetate) copolymer containing 87% vinyl chloride and 13% vinyl acetate, in which they observed that E_D remained constant for

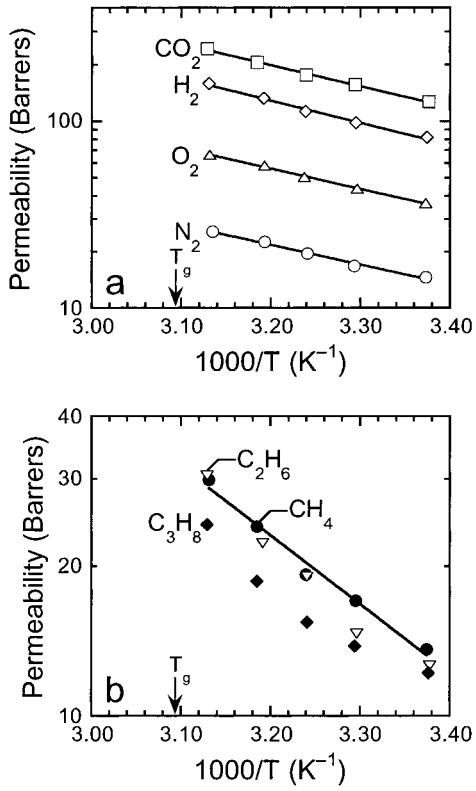

Figure 5. Temperature dependence of gas permeability coefficients for (a) permanent gases and (b) hydrocarbons in PFOMA. Shown in (a) are permeability coefficients for N_2 (○), O_2 (△), H_2 (◇), and CO_2 (□). The coefficients for CH_4 (●), C_2H_6 (▽), and C_3H_8 (◆) are displayed in (b). Solid lines correspond to least-squares regressions of eq 4 to the data (where applicable). The T_g of PFOMA is identified.

Table 4. Activation Energies of Gas Permeation (E_P, Expressed in kJ/mol) in PFOA and PFOMA

	N_2	O_2	H_2	CH_4	C_2H_6	C_3H_8	CO_2
PFOA	25 ± 1.2	20 ± 0.7	19 ± 0.2	22 ± 0.8	21 ± 0.5	13 ± 0.9	9.4 ± 0.8
PFOMA	20 ± 1.2	21 ± 0.6	23 ± 1.2	26 ± 1.9	26 ± 3.6[a]	14 ± 1.3[a]	22 ± 0.7
TFE/BDD87[b]	2.2	1.4	1.4	2.3	3.9		0.2

[a] These E_p values are estimates for the glassy state obtained by fitting eq 4 to the permeation data at 23, 30, and 35 °C. [b] Reference 51.

Table 5. Pressure-Normalized Fluxes and Selectivities of PFOA and PS-*b*-PFOA Copolymers at 35 °C, 446 kPa Feed Pressure, and 101 kPa Permeate Pressure

	pressure-normalized flux (GPU)[a]						
	N_2	O_2	H_2	CH_4	C_2H_6	C_3H_8[b]	CO_2
PFOA	41	92	220	43	51	65	350
PS-*b*-PFOA, $\phi_S = 0.12$	19	39	75	18	22	26	140
PS-*b*-PFOA, $\phi_S = 0.24$	12	30	64	14	17	20	110

[a] 1 GPU = 10^{-6} cm^3 (STP)/(cm^2·s·cmHg). [b] C_3H_8 permeability was measured at a feed pressure of 308 kPa and a permeate pressure of 101 kPa.

small penetrants (e.g., He and H_2) but decreased for the largest penetrant investigated (CO_2) below the T_g corresponding to the T_g of poly(vinyl acetate). In the present study, non-Arrhenius behavior is only observed for the largest penetrants investigated (C_2H_6 and C_3H_8), for which the probability of encountering free volume elements of sufficient size to permit diffusion is expected to increase the most upon going from the glassy to the rubbery state.[44] For C_2H_6 and C_3H_8, a rough estimate of E_P in glassy PFOMA was obtained by fitting eq 5 to the permeability data at 23, 30, and 35 °C (i.e., at temperatures below the onset of non-Arrhenius behavior.)

Table 4 presents activation energies of permeation (E_P) for PFOA and PFOMA and, for comparison, TFE/BDD87. These E_P values are estimated from the Arrhenius expression presented previously (eq 5) and are an order of magnitude higher than E_P values for TFE/BDD87. For each gas considered except CO_2, the estimated values of E_P are similar in magnitude for PFOA and PFOMA. The molecular basis for the substantially higher activation energy of permeation of CO_2 in PFOMA is not clear. Activation energies of permeation did not vary systematically with either penetrant critical volume, a convenient measure of penetrant size, or with penetrant critical temperature, a parameter often used to characterize penetrant condensability and consequently solubility.

Permeation Properties of PS-*b*-PFOA Block Copolymers. Pure gas pressure-normalized fluxes for two PS-*b*-PFOA diblock copolymers are provided in Table 5. Permeability coefficients have been calculated from the data in Table 5 using the same method discussed previously and are presented in Table 6. The uncertainty in these values is estimated to be less than 20% based on a propagation of error analysis.[32] In all cases, gas permeability coefficients of PS-*b*-PFOA copolymers lie between those of the PFOA and PS homopolymers. As the PS content of the copolymers increases, gas permeability decreases, while the ideal selectivity increases. The ideal selectivities of the PS-*b*-PFOA copolymers are similar to those of PFOA, suggesting that PFOA constitutes the transport-controlling, continuous microphase. This hypothesis is reasonable since the polymer matrix is composed primarily of PFOA.

Permeation through a structured biphasic material wherein the minor component is randomly dispersed with sharp interfaces in a continuous matrix of the major component is often described by the generalized Maxwell model:[45]

$$P_{struct} = P_c\left[1 + \frac{(1+G)\phi_d}{\left(\frac{P_d/P_c + G}{P_d/P_c - 1}\right) - \phi_d}\right] \qquad (11)$$

where P_{struct} is the permeability of the structured polymer (the PS-*b*-PFOA block copolymer in the present study), and P_c and P_d denote the continuous- and dispersed-phase permeabilities, respectively. The volume fraction of the dispersed phase is given by ϕ_d, and G is a geometric factor accounting for dispersion shape. The upper and lower bounds of the generalized Maxwell model for microphase-separated block copolymers correspond to lamellar morphologies possessing different orientations. If lamellae are oriented parallel to the direction of permeation, $G \rightarrow \infty$, and there is minimum resistance to flow. If lamellae are oriented normal to the flow direction, $G \rightarrow 0$, and maximum impedance of flow occurs due to obstructive layers of the less permeable component. Estimates of G obtained from the generalized Maxwell model (eq 11) based on the assumption that PFOA is the continuous phase are approximately 10^{-1} for N_2, O_2, CH_4, and CO_2. These results suggest that the morphology of these nanostructured materials is consistent with a highly defective, laminate composite structure in which PS microdomains are oriented perpendicular to the direction of permeation. In this case, the PS-rich regions impede gas flow through the material, resulting in reduced gas permeabilities. However, since these microdomains do not appear to be fully connected, the selectivities are governed by the more permeable PFOA phase. Even if

Table 6. Gas Permeability Coefficients and Selectivities of PFOA, PS, and PS-*b*-PFOA Copolymers at 35 °C, 446 kPa Feed Pressure, and 101 kPa Permeate Pressure

	permeability coefficient (barrers)							selectivity		
	N_2	O_2	H_2	CH_4	C_2H_6	C_3H_8[a]	CO_2	O_2/N_2	H_2/CH_4	CO_2/CH_4
PFOA	70	160	370	73	87	110	590	2.3	5.1	8.1
PS-*b*-PFOA, $\phi_S = 0.12$[c]	23	47	90	22	27	31	170	2.0	4.0	7.7
PS-*b*-PFOA, $\phi_S = 0.24$[d]	19	45	96	21	26	30	170	2.4	4.6	8.1
PS[b]	0.53[52]	2.9[52]	22.6[31]	0.79[52]			12.4[52]	5.5	29	16

[a] C_3H_8 data were collected at a feed pressure of 308 kPa and a permeate pressure of 101 kPa. [b] PS permeability coefficients were determined at 1 atm. [c] Based on estimated separating layer thickness of 1.2 ± 0.2 μm. [d] Based on estimated separating layer thickness of 1.5 ± 0.2 μm.

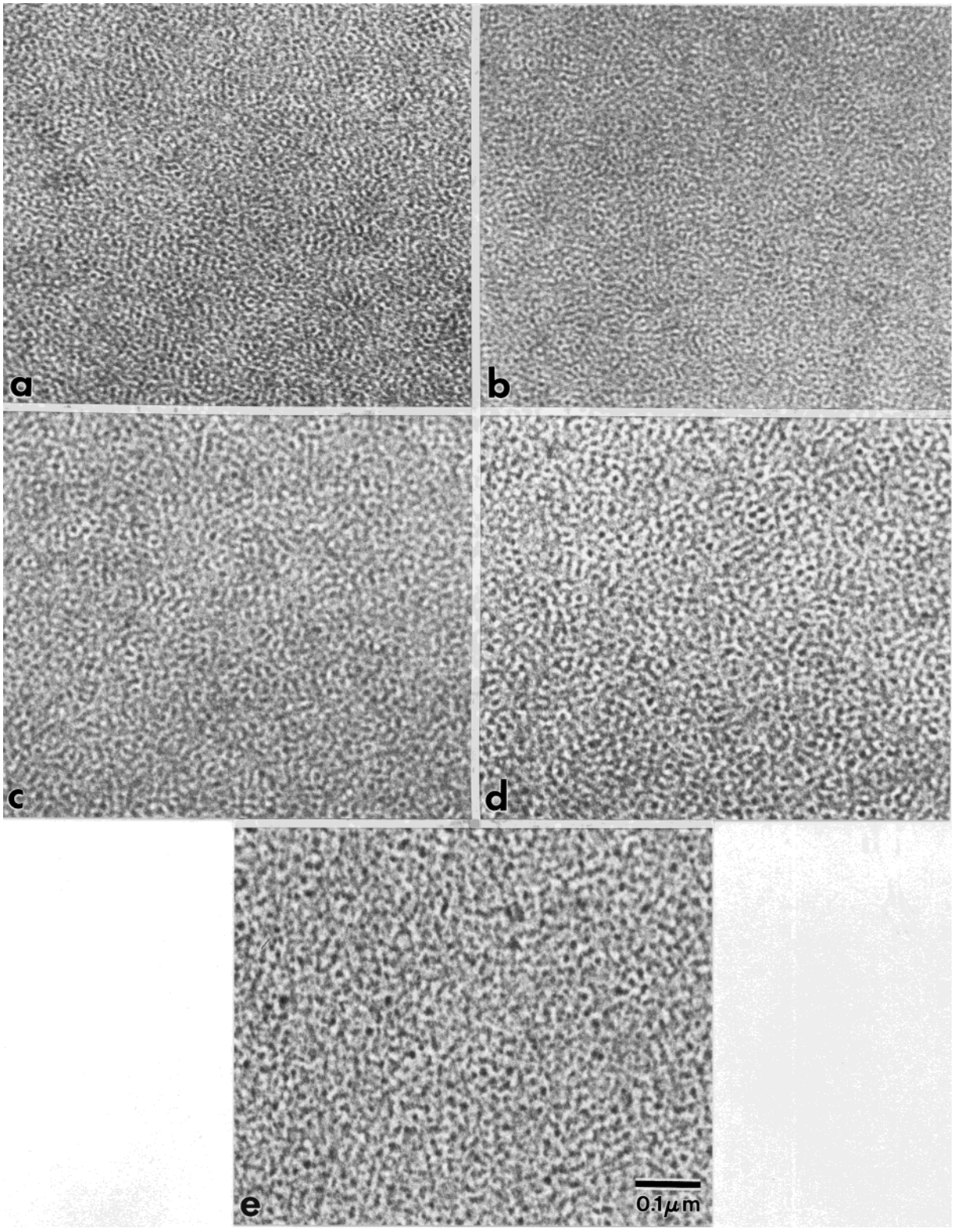

Figure 6. Transmission electron micrographs of PS-*b*-PFOA diblock copolymers in which the PS microdomains appear dark due to selective staining. All the copolymers consist of a PS block with $\bar{M}_n = 3700$, whereas the $\bar{M}_n$ of the PFOA block is varied as follows: (a) 13 700, (b) 27 500, (c) 39 800, (d) 61 200, and (e) 244 500. The corresponding PS volume fractions (ϕ_S) of these copolymers are (a) 0.31, (b) 0.18, (c) 0.13, (d) 0.09, and (e) 0.02.

the PS domains were fully connected to form a co-continuous structure, PS permeability coefficients are so much lower than those of PFOA that the separation properties of the sample would still be governed by those of PFOA because most of the gas permeation would occur through PFOA-rich regions.

Morphological Characteristics of PS-*b*-PFOA Block Copolymers. Transmission electron micrographs of five PS-*b*-PFOA copolymers composed of PS blocks of constant $\bar{M}_n$ (3700) and PFOA blocks differing in $\bar{M}_n$ (from 13 700 to 244 500) are displayed in Figure 6. In these images, the PS microdomains appear electron-

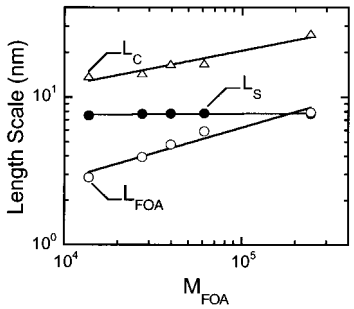

Figure 7. Variation of L_S (●), L_{FOA} (○), and L_c (△) with M_{FOA} on double-logarithmic coordinates for the five PS-*b*-PFOA diblock copolymers displayed in Figure 6. The solid lines are power-law fits to the data, and their slopes yield the values of α reported in the text.

opaque (dark) due to selective RuO_4 staining. The copolymers with PFOA blocks of $\bar{M}_n$ = 27 500 and 39 800, shown in parts b and c of Figure 6, respectively, consist of 18 and 13 vol% PS and are similar in composition to the block copolymers used in the gas permeation studies (ϕ_S = 0.24 and 0.12). Since the morphologies in these micrographs confirm that the copolymers are microphase-separated but do not resemble any of the established (classical or complex) morphologies (despite the slow solvent evaporation procedure employed during preparation), it is reasonable to expect that the copolymers used in the permeation studies possess similar, but possibly more refined, morphologies (due to their higher $\bar{M}_n$) than those in Figure 6b,c. No evidence of long-range order exists in any of these materials, most likely due to their molecular weight *and* (anticipated) compositional polydispersity.[46] At each composition, the PFOA microphase appears continuous. In particular, regions of co-continuous PS and PFOA channels exist in Figure 6b,c, suggesting that these morphologies may exhibit bicontinuity.[47] Such nanostructures are also consistent with the highly defective lamellar morphology previously inferred from the permeation results.

The characteristic dimensions of the morphologies displayed in Figure 6 are presented in Figure 7 and include the average thicknesses of the PS and PFOA microdomains (L_S and L_{FOA}, respectively) acquired from real-space measurements, as well as the average correlation length (L_c) derived from the correlation maxima in 2D Fourier transforms of the images. These dimensions are presented on double-logarithmic coordinates as a function of the PFOA block mass (M_{FOA}) in Figure 7. As expected from the molecular characteristics of these copolymers, L_S remains invariant with respect to M_{FOA}, since the PS block mass (M_S) does not vary in the copolymer series. In contrast, L_{FOA} is seen to increase with increasing M_{FOA}. It immediately follows (and is observed) that L_c likewise increases with an increase in M_{FOA}. The relationships evident in Figure 7 therefore correctly reflect the variation in molecular characteristics of the copolymers investigated in this work. Closer examination of the dependence of these dimensions on molecular weight may provide insight into the extent of molecular anisotropy.

Block copolymers exhibit three ordered regimes determined by the degree of block segregation: strong, intermediate, and weak. A convenient measure of these segregation regimes is the thermodynamic incompatibility, designated χN, where χ denotes the Flory–Huggins interaction parameter and N is the number of statistical units along the copolymer backbone. Within these regimes, the blocks stretch to different extents, and the extent of block stretching governs the characteristic dimensions of the microphase-separated morphologies. The data in Figure 7 reveal that both L_{FOA} and L_c increase as M_{FOA}^{α}, where α is equal to 0.34 ± 0.01 for L_{FOA} and 0.24 ± 0.01 for L_c. In contrast, L_S remains relatively constant at about 7.7 nm. Since the gyration diameter (D_g) of unperturbed PS with $\bar{M}_n$ = 3700 is estimated to be ca. 3.4 nm,[48] the PS microdomains correspond to about $2.2D_g$ in thickness, indicating that the PS blocks are slightly stretched along the interfacial normal.

Since α provides a measure of the degree of block stretching, it could, in principle, be used to assign copolymers to one of the segregation regimes listed above. According to recent theoretical considerations,[49] values of α for ordered monomolecular copolymers are predicted to be about 0.67 in the strong-segregation regime, 0.80 in the intermediate-segregation regime, and 0.99 in the weak-segregation regime. The values of α derived from L_{FOA} and L_c in Figure 7 for the PS-*b*-PFOA copolymers do not match, however, any of these predicted scaling exponents. This disagreement may be due to copolymer material considerations (e.g., molecular or compositional polydispersity), in which chain packing and interfacial curvature vary due to local differences in block length. Another, more likely explanation for the apparent disagreement with theory is attributed to overlap of projected PS microdomains in the TEM images. Since the PS microdomains are significantly smaller (ca. 7.7 nm) than a typical TEM section (ca. 100 nm), each TEM image constitutes a projection through several microdomain layers. The resultant superimposed image complicates conventional analysis of α. Thus, we conclude that the values of α measured here cannot be used to discern the segregation regime in which these PS-*b*-PFOA copolymers reside. Because of uncertainties in the value of χ between PS and PFOA and the impact of molecular weight/compositional polydispersity on χ, no attempt is likewise made to estimate the magnitude of χN for these copolymers.

Reexamination of the DSC data provided in Table 1, coupled with the T_g calculations provided earlier in this work, reveals that the T_g's of some of the PS blocks are depressed below what is expected on the basis of molecular weight. In contrast, the T_g's of the PFOA blocks differ only slightly from that of the PFOA homopolymer. These two observations taken together suggest that the PS microdomains are not completely demixed. While it remains uncertain at this time whether such residual mixing is attributed to thermodynamic or kinetic considerations (or a combination thereof), the existence of residual mixing in a microphase-separated block copolymer strongly suggests that χN is depressed relative to a highly demixed copolymer in the strong-segregation regime.

Conclusions

The temperature-dependent permeation properties of PFOA, PFOMA, and PS-*b*-PFOA diblock copolymers are reported for a family of gases. In general, PFOMA possesses lower gas permeabilities and higher selectivities than PFOA, which is consistent with its lower fractional free volume and, based on T_g, more restricted chain mobility. The activation energy of permeation for PFOMA increases for larger penetrants (e.g., C_2H_6 and

C_3H_8) as T_g is approached from below. For small penetrants, such as N_2 and O_2, no change in E_P is observed near T_g. The permeation and morphological characteristics of PS-*b*-PFOA diblock copolymers have also been investigated. The PS-*b*-PFOA copolymers exhibit microphase-separated morphologies with no evidence of long-range order, which is attributed to the molecular weight/compositional polydispersity of the copolymer molecules. These copolymers possess gas permeabilities intermediate between those of rubbery, highly permeable PFOA and glassy, relatively impermeable PS, and the permeability coefficients decrease with increasing PS content. The gas permeabilities and selectivities suggest that the morphologies are highly defective laminate structures and are consistent with results from electron microscopy.

Acknowledgment. This work was supported in part by the Office of Naval Research, the National Science Foundation (Presidential Faculty Fellowship: J. M. D. 1993−1997), and the STC program of the National Science Foundation under Agreement No. CHE9876674. We thank M. Gregory of the NCSU Analytical Instrumentation Facility for technical assistance.

References and Notes

(1) DeSimone, J. M.; Guan, Z.; Elsbernd, C. S. *Science* **1992**, *257*, 945.
(2) Emissions of greenhouse gases in the United States, Energy Information Administration, DOE/EIA-0573(96), Washington, DC, Oct 1997.
(3) Wall, L. A. *Fluoropolymers*; John Wiley & Sons: New York, 1972.
(4) Guan, Z.; Elsbernd, C. S.; DeSimone, J. M. *Polym. Prepr. (Am. Chem. Soc., Div. Polym. Chem.)* **1992**, *33*, 329.
(5) Guan, Z.; DeSimone, J. M. *Macromolecules* **1994**, *27*, 5527.
(6) Spontak, R. J.; Alexandridis, P. *Curr. Opin. Colloid Interface Sci.* **1999**, *4*, 140.
(7) Bates, F. S.; Fredrickson, G. H. *Phys. Today* **1999**, *52*, 32.
(8) Bondar, V. I.; Freeman, B. D.; Pinnau, I. *J. Polym. Sci., Part B: Polym. Phys.* **1999**, *37*, 2463.
(9) Csernica, J.; Baddour, R. F.; Cohen, R. E. *Macromolecules* **1989**, *22*, 1493.
(10) Csernica, J.; Baddour, R. F.; Cohen, R. E. *Macromolecules* **1990**, *23*, 1429.
(11) Rein, D. H.; Csernica, J.; Baddour, R. F.; Cohen, R. E. *Macromolecules* **1990**, *23*, 4456.
(12) Rein, D. H.; Baddour, R. F.; Cohen, R. E. *J. Appl. Polym. Sci.* **1992**, *45*, 1223.
(13) Sax, J. E.; Ottino, J. M. *Polymer* **1985**, *26*, 1073.
(14) Shah, N.; Sax, J. E.; Ottino, J. M. *Polymer* **1985**, *26*, 1239.
(15) Koshimura, K.; Sato, H. *Polym. Bull.* **1992**, *29*, 705.
(16) Odani, H.; Taira, K.; Nemoto, N.; Kurata, M. *Bull. Inst. Chem. Res.* **1975**, *53*, 216.
(17) Sukhanova, T. Y.; Kuznetsov, Y. P.; Kruchinina, Y. V.; Lukashova, N. V.; Sidorovich, A. V.; Gusinskaya, V. A.; Peltsbauer, Z. *Polym. Sci. U.S.S.R. (Engl. Transl.)* **1989**, *31*, 2741.
(18) Tsujita, Y.; Yoshimura, K.; Yoshimizu, H.; Takizawa, A.; Kinoshita, T.; Furukawa, M.; Yamada, Y.; Wada, K. *Polymer* **1993**, *34*, 2597.
(19) Ghosal, K.; Freeman, B. *Polym. Adv. Technol.* **1994**, *5*, 673.
(20) Graham, T. *London Edinburgh Dublin Philos. Mag. J. Sci.* **1866**, *32*, 401.
(21) Meares, P. *J. Am. Chem. Soc.* **1954**, *76*, 3415.
(22) Otsu, T.; Kuriyama, A. *Polym. Bull.* **1984**, *11*, 135.
(23) Otsu, T.; Kuriyama, A. *Polym. J.* **1985**, *17*, 97.
(24) Betts, D. E. Ph.D. Dissertation, The University of North Carolina at Chapel Hill, 1998.
(25) Crank, J.; Park, G. S. In *Diffusion in Polymers*; Crank, J., Park, G. S., Eds.; Academic: New York, 1968; p 452.
(26) Stern, S. A.; Gareis, P. J.; Sinclair, T. F.; Mohr, P. H. *J. Appl. Polym. Sci.* **1963**, *7*, 2035.
(27) Utracki, L. A. *Polymer Alloys and Blends*; Hanser: Berlin, 1990.
(28) Kane, L.; Satkowski, M. M.; Smith, S. D.; Spontak, R. J. *J. Polym. Sci., Polym. Phys. Ed.* **1997**, *35*, 2653.
(29) Lu, X.; Jiang, B. *Polymer* **1991**, *32*, 471.
(30) Resnick, P. R.; Buck, W. H. In *Modern Fluoropolymers*; Scheirs, J., Ed.; John Wiley & Sons: New York, 1997; p 397.
(31) Pauly, S. In *Polymer Handbook*; Brandrup, J., Immergut, E., Eds.; John Wiley and Sons: New York, 1989; p VI/435.
(32) Bevington, P. R.; Robinson, D. K. *Data Reduction and Error Analysis for the Physical Sciences*, 2nd ed.; McGraw-Hill: New York, 1992.
(33) Freeman, B. D.; Pinnau, I. In *Polymer Membranes for Gas and Vapor Separations: Chemistry and Materials Science*; Freeman, B. D., Pinnau, I., Eds.; ACS Symp. Ser.; American Chemical Society: Washington, DC, 1999; Vol. 733, p 1.
(34) Bondi, A. *J. Phys. Chem.* **1964**, *68*, 441.
(35) Pinnau, I.; Toy, L. G. *J. Membr. Sci.* **1996**, *109*, 125.
(36) Van Krevelen, D. W. *Properties of Polymers*, 3rd ed.; Elsevier Science: Amsterdam, The Netherlands, 1990.
(37) Vieth, W. R. *Diffusion In and Through Polymers*; Hanser: New York, 1991.
(38) Koo, G. P. In *Fluoropolymers*; Wall, L. A., Ed.; John Wiley & Sons: New York, 1972; Vol. XXV, p 507.
(39) Koros, W. J.; Hellums, M. W. In *Encyclopedia of Polymer Science and Engineering*; Kroschwitz, J. I., Ed.; John Wiley & Sons: New York, 1990; p 1211.
(40) Robeson, L. M. *J. Membr. Sci.* **1991**, *62*, 165.
(41) Freeman, B. D. *Macromolecules* **1998**, *32*, 375.
(42) Baker, R. W. *Membrane Technology and Applications*; McGraw-Hill: New York, 2000.
(43) Kumins, C. A.; Roteman, J. *J. Polym. Sci.* **1961**, *55*, 683.
(44) Stannett, V. In *Diffusion in Polymers*; Crank, J., Park, G. S., Eds.; Academic: New York, 1968; p 41.
(45) Petropoulos, J. H. *J. Polym. Phys., Polym. Phys. Ed.* **1985**, *23*, 1309.
(46) Burger, C.; Ruland, W.; Semenov, A. N. *Macromolecules* **1990**, *23*, 3339.
(47) Hashimoto, T.; Koizumi, S.; Hasegawa, H.; Isumitani, T.; Hyde, S. T. *Macromolecules* **1992**, *25*, 1433.
(48) Jinnai, H.; Nishikawa, Y.; Spontak, R. J.; Smith, S. D.; Agard, D. A.; Hashimoto, T. *Phys. Rev. Lett.* **2000**, *84*, 518.
(49) Matsen, M. W.; Bates, F. S. *Macromolecules* **1996**, *29*, 1091.
(50) Rudd, J. F. In *Polymer Handbook*, 3rd ed.; Brandrup, J., Immergut, E. H., Eds.; John Wiley & Sons: New York, 1989; p V/81.
(51) Merkel, T. C.; Bondar, V.; Nagai, K.; Freeman, B. D.; Yampolskii, Y. P. *Macromolecules* **1999**, *32*, 8247.
(52) Puleo, A. C.; Murganandam, N.; Paul, D. R. *J. Polym. Sci., Polym. Phys. Ed.* **1989**, *27*, 2385.

MA010355I